COMPUTER CALCULATIONS OF CROSS SECTIONS FOR ELECTRON IMPACT IONIZATION OF HELIUM

An abstract of a Thesis by
Bruce M. Bakken
June 1977
Drake University
Advisor: Dr. Donald H. Madison

Triple differential cross sections for electron-impact ionization of helium are calculated in the distorted wave approximation. The distorted wave formalism is discussed for the z-axis parallel to the momentum transfer direction. Problems associated with programming this formalism are outlined. The cross sections are then compared to experimental results and other theoretical calculations.

COMPUTER CALCULATIONS OF CROSS SECTIONS FOR ELECTRON IMPACT IONIZATION OF HELIUM

A Thesis

Presented to

The School of Graduate Studies

Drake University

In Partial Fulfillment

of the Requirements for the Degree

Master of Science

---

by

Bruce M. Bakken

June 1977

COMPUTER CALCULATIONS OF CROSS SECTIONS FOR ELECTRON IMPACT IONIZATION OF HELIUM

by

Bruce M. Bakken

Approved by Committee:

Dr. Don H. Madison
Chairperson

Dr. Robert W. Lutz

Dr. Michael J. Folk

Dr. Earle L. Canfield
Dean of the School of Graduate Studies

TABLE OF CONTENTS

Page

LIST OF TABLES iv

LIST OF FIGURES v

Chapter

1. INTRODUCTION 1

2. THEORY 6

3. RESULTS 13

4. CONCLUSIONS 29

REFERENCES 30

APPENDIX A 31

APPENDIX B 34

APPENDIX C 40

APPENDIX D 45

APPENDIX E 51

LIST OF TABLES

Table		Page
1.	Comparison of cross sections in units of $a_o^2/Sr^2/Ry$ for Z along $\bar{q}$ to the interpolated cross sections for Z along $\bar{K}_i$ of Madison *et al*.	14
2.	Table of cross sections for Z along $\bar{q}$ in units of $a_o^2/Sr^2/Ry$, for comparison of partial wave parameters.	52

LIST OF FIGURES

Figure		Page
1.	Sketch of the coordinate system for electron impact ionization with the Z axis oriented along the axis of incident particles.	4
2.	Sketch of the coordinate system for electron impact ionization with the Z axis oriented along the axis of momentum transfer.	19
3.	Triple Differential Cross Sections for 100 eV electron impact ionization of helium in units of $a_o^2/Sr^2/Ry$. The experimental data are those of Beatty, et al., the solid curve is the present DWA calculation; the dotted curve is the PWBA calculation and the dashed curve is the CPBA calculation. The angle of observation of the faster electron, θ_f, is 20° and the energy of the slower electron, E_s, is 5 eV. The cross sections are for Φ=0 to 180° for a cone of half angle θ_s=45°.	21
4.	Same as Figure 3 except E_i=105 eV and E_s=10 eV.	23
5.	Same as Figure 3 except E_i=125 eV, E_s=30 eV, and the cone is now centered about θ_s=30°.	25
6.	Same as Figure 3 except E_i=165 eV, E_s=70 eV, and the cone is now centered about θ_s=25°.	27

Chapter 1

INTRODUCTION

The problem of atomic charged particle scattering has been studied experimentally and theoretically since the 1920's. Until recently, first order approximations, such as the Plane Wave Born Approximation (PWBA) have yielded satisfactory results. However, with improved experimental techniques, detailed measurements of ionization cross sections have revealed structure that these first order theories cannot adequately explain. Recently, Erhardt et al.,[1-4] Hood et al.,[5] and Weigold[6] have measured triple differential cross sections for electron impact ionization. Various theoretical calculations for this process have been performed in the PWBA,[7-10] the Coulomb Projected Born Approximation (CPBA),[11] the many body Green's function approach,[12] and the Distorted Wave Approximation (DWA).[13] It has been shown that the distorted wave approach gives theoretical results that are in better agreement with the experimental data.

The triple differential cross sections predicted by the PWBA are azymuthally symmetric in a cone about the axis of momentum transfer $\bar{q} = \bar{K}_i - \bar{K}_f$, where $\bar{K}_i$ and $\bar{K}_f$ are the wave number vectors of the incident and fast final state electrons respectively. Since the PWBA continues to be a standard reference, it is interesting to examine the behavior of

cross sections in the DWA expressed relative to the q axis. Inasmuch as the previous DWA calculations were performed for the Z axis oriented along $\bar{K}_i$, the cross sections for the cone about $\bar{q}$ could not readily be obtained. The subject of this thesis entails writing a computer program to calculate triple differential cross sections for electron impact ionization of helium for the cone about q in the distorted wave approximation. The theory for the calculation in this rotated frame has been presented by Madison et al.[13]

The physical phenomena connected with electron impact ionization can be described as follows: an electron with energy E_i is incident on an atom initially at rest. The electron and the atom interact, scattering the incident electron and ejecting one of the atomic electrons, as shown in Figure 1. The scattering plane is defined by the momentum vectors of the incident and final faster electron. The kinematic quantities of interest are the angle of observation of the faster electron in the scattering plane, θ_f, the solid angle of observation of the slower electron, θ_s, Φ_s, and the energy of the slower electron E_s. Conservation of energy uniquely determines the energy of the faster electron. For such atomic scattering processes, a cross section is defined as the number of particles found at the two electron detectors divided by the incident flux.

In this thesis, the general theory of the distorted wave approximation for this process as derived by

Figure 1. Sketch of the coordinate system for electron impact ionization with the Z axis oriented along the axis of incident particles.

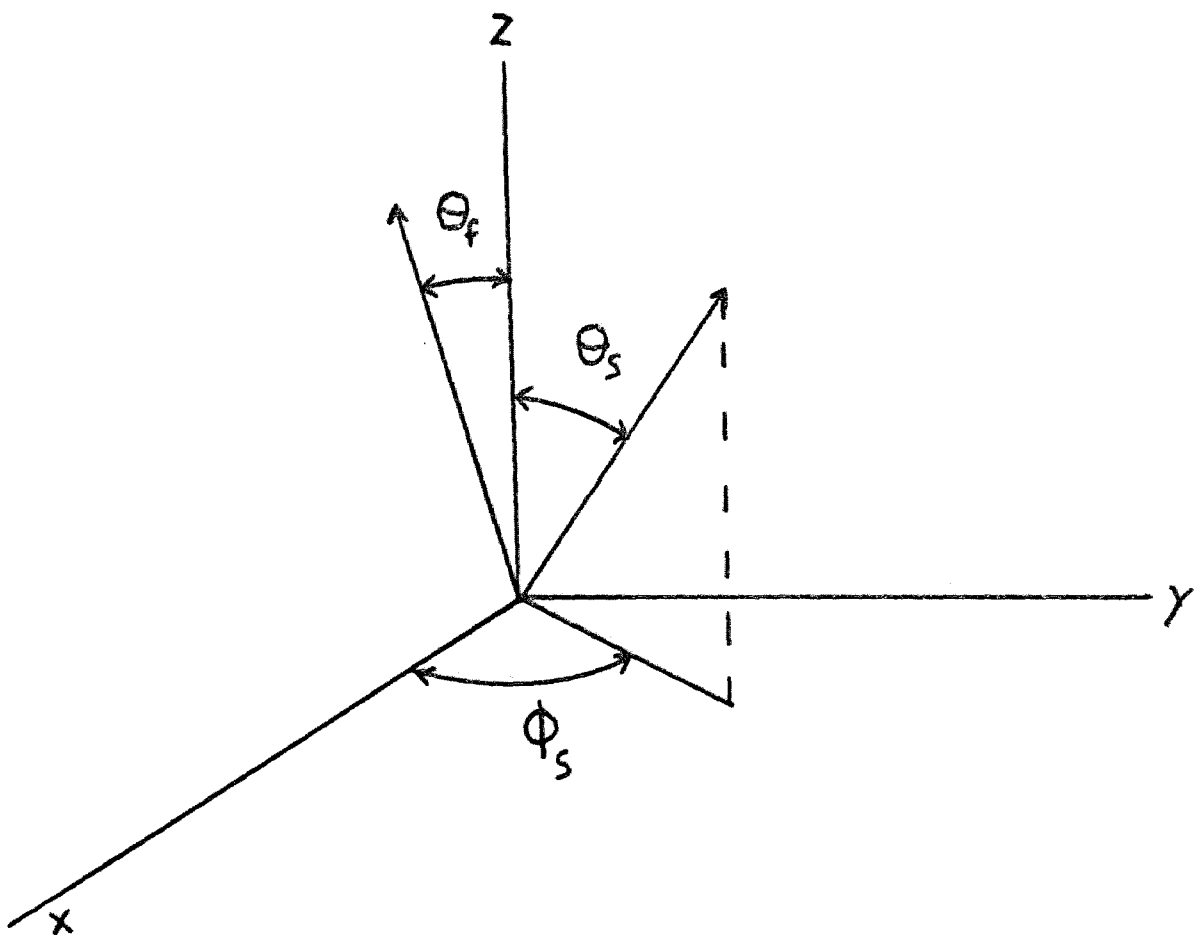

Figure 1

Madison et al.[13] will be discussed, the problems encountered in implementing the theory with a computer program will be outlined, and the results will be compared to other theoretical approximations and the experimental results of Beatty et al.[14]

Chapter 2

THEORY

In the notation used in this thesis, the triple differential cross section is denoted by $\frac{d\sigma}{d\Omega_f d\Omega_s dE}$, where Ω_f and Ω_s are the solid angles of the detector for the fast and slow electrons respectively, and E is the energy of the ejected electron. According to Madison et al.[13]

$$\frac{d\sigma}{d\Omega_f d\Omega_s dE} = |f|^2 + |g|^2 - Re(f^*g) \qquad (1)$$

where f and g are the direct and exchange amplitudes respectively. These amplitudes may be written as

$$f = (4\pi^3)^{-1} (k_i k_s k_f)^{-\frac{1}{2}} \sum_{\ell_s m_s} D^{\ell_o m_o}_{\ell_s m_s}(\theta_f) P^{|m_s|}_{\ell_s}(\theta_s) e^{i m_s \phi_s} \qquad (2)$$

and

$$g = (4\pi^3)^{-1} (k_i k_s k_f)^{-\frac{1}{2}} \sum_{\ell_f m_f} E^{\ell_o m_o}_{\ell_f m_f}(\theta_f) P^{|m_f|}_{\ell_f}(\theta_s) e^{i m_f \phi_s} \qquad (3)$$

where P^m_ℓ is an associated Legendre polynomial, and where $D^{\ell_o m_o}_{\ell_s m_s}(\theta_f)$ and $E^{\ell_o m_o}_{\ell_f m_f}(\theta_f)$ are the direct and exchange amplitude coefficients respectively. For the direct (exchange) case, the scattered (ejected) electron is the fast electron, while the ejected (scattered) electron is the slow electron. Consistent with the fast and slow notation, the angular momentum quantum numbers for the effected

electron are denoted by $\ell_s(\ell_f)$ for the direct (exchange) case and ℓ_o and m_o are the angular momentum quantum numbers for the ground state of the atom. For the case of electron impact ionization of helium, the atom is in a singlet S state; hence $\ell_o=m_o=0$.

The expressions for $D^{0\ 0}_{\ell_s m_s}(\theta_f)$ and $E^{0\ 0}_{\ell_f m_f}(\theta_f)$ depend on the choice of coordinate system. As discussed earlier, in this problem the Z axis is oriented along the axis of momentum transfer. For this orientation the direct and exchange amplitude coefficients are given by the following expressions:

$$D^{0\ 0}_{\ell_s m_s} = \sum_{\substack{\ell_i \ell_f \\ m_f}} \frac{\hat{\ell}_i^{\,2}\hat{\ell}_f^{\,2}}{\hat{\ell}_s^{\,2}}\, i^{(\ell_i-\ell_f-\ell_s)}\,(-1)^{[2m_s+|m_f|+|m_s|+|m_s-m_f|]/2}$$

$$\times\ I^{k_i k_f k_s}_{o\ell_i\ell_f\ell_s}\ C(\ell_i,\ell_f,\ell_s;m_s-m_f,m_f,m_s)\ C(\ell_i,\ell_f,\ell_s;0,0,0)$$

$$\times\ R^{|m_f|}_{\ell_f}\ R^{|m_s|}_{\ell_s}\ R^{|m_s-m_f|}_{\ell_i}\ P^{|m_f|}_{\ell_f}(\beta)\ P^{|m_s-m_f|}_{\ell_i}(\alpha) \qquad (4)$$

and

$$E^{0\ 0}_{\ell_f m_f} = \sum_{\substack{\ell_i \ell_s \\ m_s}} \frac{\hat{\ell}_i^{\,2}\hat{\ell}_f^{\,2}}{\hat{\ell}_s^{\,2}}\, i^{(\ell_i-\ell_f-\ell_s)}\,(-1)^{[2m_s+|m_f|+|m_s|+|m_s-m_f|]/2}$$

$$\times\ C(\ell_i,\ell_f,\ell_s,m_s+m_f,-m_f,m_s)\ C(\ell_i,\ell_f,\ell_s;0,0,0)\ I^{k_i k_s k_f}_{o\ell_i\ell_s\ell_f}$$

$$\times\ R^{|m_f|}_{\ell_f}\ R^{|m_s|}_{\ell_s}\ R^{|m_s+m_f|}_{\ell_i}\ P^{|m_s+m_f|}_{\ell_i}(\alpha)\ P^{|m_s|}_{\ell_s}(\beta) \qquad (5)$$

where α is the angle between $\bar{K}_i$ and $\bar{q}$, $\beta = \alpha + \theta_f$,

$$R_\ell^{|m|} = \left[\frac{(\ell-|m|)!}{(\ell+|m|)!}\right]^{\frac{1}{2}}$$

and C is a Clebsch-Gordon coefficient.[15] $I_{o\ell_i\ell_f\ell_s}^{k_i k_f k_s}$ is an overlap integral defined as follows:

$$I_{o\ell_i\ell_m\ell_n}^{k_i k_m k_n} = \int_o^\infty \beta_{\ell_m}(k_m R)\beta_{\ell_i}(k_i R) F_{o\ell_n}^{k_n}(R)\,dR \tag{6}$$

where

$$F_{o\ell_n}^{k_n}(R) = \int_o^\infty \beta_{\ell_n}(k_n r)\,\frac{r_<^\ell}{r_>^{\ell+1}}\,U_{\ell_o}(r)\,dr \tag{7}$$

and β_n, β_m and β_i are solutions to the radial Schrodinger equation,

$$-\frac{\hbar^2}{2m}\frac{d^2\beta}{dr^2} + \left[\frac{\hbar^2(\ell(\ell+1))}{2m\,r^2} + V(r)\right]\beta = E\beta \tag{8}$$

such that for the direct case, n=s and m=f, and for the exchange case n=f and m=s. In this calculation, it is assumed that the fast electron is effectively scattered by the neutral atom, and the slow final state electron is scattered by the ion. As a result, the atomic potential V(r) used for the incident and fast final state electron in the radial Schrodinger equation is a numerical Hartree Fock potential[16] for neutral helium which approaches zero asymptotically. The potential used for the slow electron is a Hartree Fock potential which approaches a Coulomb potential asymptotically. $U_o(r)$ is the bound state wave

function of the helium atom obtained from the neutral Hartree Fock calculations.

In the radial Schrodinger equation, the angular momentum barrier, $\frac{\hbar^2 \ell(\ell+1)}{2m\ r^2}$ provides a region around the nucleus into which the electron cannot effectively penetrate. For high values of angular momentum the range of this barrier becomes greater than the effective range of the atomic potential. Partial waves with large angular momenta may be approximated by spherical Bessel functions, which are the solutions to the radial Schrodinger equation for V=0. A cutoff angular momentum, ℓ_c, may then be defined as the angular momentum for which the numerical partial waves may be replaced by spherical Bessel functions. For values of r greater than the range of the atomic potential, the form factor integral in equation 7 is merely a constant divided by r. $I^{k_i k_f k_s}_{o \ell_i \ell_f \ell_s}$ is then an integral of two spherical Bessel functions divided by the radius. This integral may be done analytically and the result can be expressed in terms of hypergeometric functions. Consequently, the overlap integral can be calculated analytically in the direct case for $\ell_i > \ell_c$. It should be noted that for $\ell_i > \ell_c$, the DWA amplitude becomes the PWBA amplitude. Obviously, this method cannot be used for the exchange amplitude, since the roles of the electrons are reversed and the integral of equation 6 contains a Coulomb wave function. In these calculations, the value of ℓ_c is about 20.

Since a computer program to calculate $I^{k_i k_f k_s}_{o\ell_i \ell_f \ell_s}$ is available from previous work,[13] this task consisted of writing a FORTRAN program to calculate the direct and exchange amplitude coefficients, the direct and exchange amplitudes and finally, the cross sections. Flow charts for the program, the direct and exchange amplitude coefficient calculators and the amplitude and cross section calculator are displayed in Appendices A through D, respectively.

Due to the complexity of the algorithms used, careful attention must be paid to numerical stability. Large values of ℓ_f and m_f introduce particular difficulty in the calculation of the associated Legendre polynomials due to the iterative procedure used in that routine. Other difficulties arise due to the size of the problem. In the direct and exchange coefficient calculators alone, for an average run, over five million calculations are performed. Of these calculations, roughly one million are calls to subroutines. Due to a limited amount of core storage, over 500 complex arrays had to be stored on mass storage devices.

In writing a complicated routine with many nested DO loops to compute the various summations, the order of the loops must be carefully planned. In the routine to calculate the overlap integrals, the integrals are stored as a function of ℓ_s and m_s, thus they must be referenced as a function of ℓ_s and m_s. This dictates that the outermost loop be the

loop for ℓ_s and the first nested loop be the loop for m_s, which runs from $-\ell_s$ to $+\ell_s$. Even though the summation in equation 4 does not have either ℓ_s or m_s as indices, these loops must be the outermost loops as the final result is stored as a function of ℓ_s and m_s.

The summation itself begins with a loop over the index ℓ_f, which has values ranging from zero to some maximum value set arbitrarily. The optimum maximum values for ℓ_f and ℓ_s will be discussed later. The loop over ℓ_f also contains an m_f loop ranging from $-\ell_f$ to $+\ell_f$. However, before the m_f loop, a loop over ℓ_i was incorporated. The index ℓ_i runs from $|\ell_s-\ell_f|$ to $\ell_s+\ell_f$ incremented by two due to the parity of the Clebsch-Gordon coefficient. To maximize the efficiency of the program, variables not depending on m_f are calculated outside that loop. These variables included an associated Legendre polynomial and a Clebsch-Gordon coefficient. All other parameters in the calculation depend in one way or another on m_f, including an additional associated Legendre polynomial and Clebsch-Gordon coefficient. These terms are collected, multiplied, and stored for later use by the cross section routine.

The order of the nesting of the loops is critical in terms of economy of machine time. If the loops are nested in reverse order, the associated Legendre polynomial subroutine will be called approximately eight million times. Using the nesting scheme as described above, the associated

Legendre polynomial subroutine is called about 164,000 times.

The routine for the exchange amplitude coefficient is almost exactly the same as the routine for the direct amplitude coefficient with one major exception: the roles of $\ell_f m_f$ and $\ell_s m_s$ are reversed. The summation is now performed over the indices ℓ_s and m_s, and the coefficient must be stored as a function of ℓ_f and m_f. Even with these conditions, the ℓ_s loop must still be the outermost loop since the overlap integrals are read into the routine as a function of ℓ_s and m_s. This necessitates a backward summing technique such that the final results are written as a function of the inner loop indices.

One problem encountered in the programming involved the storage of over 500 complex arrays. Since all available core memory was being utilized, a convenient technique of saving information on mass storage was needed. A sequential writing process was not convenient since accessing the overlap integrals required a nonsequential usage and reusage of various blocks of data. A subroutine was needed that could read and write arrays on mass storage such that each element of the array could be accessed by an appropriate index. The Control Data Fortran Extended library subroutines READMS and WRITMS have these features and their incorporation into the routines solved the storage problem.

Chapter 3

RESULTS

Once the program was written and debugged, testing for correctness began. The best test for correctness was to reproduce the earlier results of Madison et al.[13] For this comparison, the following parameters were used: E_i = 256.5 eV, E_s = 50 eV, θ_f = 8°, ℓ_i = 98, ℓ_c = 40, ℓ_s = 7 for the direct case, and ℓ_i = 30, and ℓ_s = 12 for the exchange case. The results of this calculation could not be compared directly to the results of Madison due to the rotation of the Z axis from $\bar{K}_i$ to $\bar{q}$. However, an easy comparison can be made in the scattering plane where the cross sections are simply shifted linearly by the angle between $\bar{K}_i$ and $\bar{q}$. For the above parameters, this angle was 35.26°. A linear interpolation was then performed for Z along K_i and compared directly to the results for Z along q. The results are shown in Table 1. Clearly, both calculations yield the same results.

Once the program had been checked, the optimum number of partial waves needed for proper convergence of the cross sections had to be obtained. Since comparisons were to be made with the experimental results of Beatty et al.,[14] the appropriate optimum maximum ℓ-values for $E_i \gtrsim 100$ eV were required. These optimum ℓ-values are found as follows: all but one of the partial wave parameters are kept constant,

Table 1

Comparison of Cross Sections in Units of $a_o^2/Sr^2/Ry$ for Z Along $\bar{q}$ to the Interpolated Cross Sections for Z Along $\bar{K}_i$ of Madison et al.

θ	Q axis	K axis (interpolated)
	For $\phi = 0°$	
0	4.927×10^{-4}	4.927×10^{-4}
10	6.762	6.761
20	7.768	7.766
30	6.581	6.581
40	3.664	3.665
50	1.373	1.374
60	.817	.818
70	1.108	1.108
80	1.257	1.257
90	1.101	1.101
100	.911	.911
110	.846	.846
120	.903	.903
130	1.026	1.025
140	1.162	1.162
150	1.268	1.269
160	1.326	1.326
170	1.340	1.340
180	1.328	1.328
	For $\phi = 180°$	
0	4.926×10^{-4}	4.926×10^{-4}
10	3.412	3.412
20	2.256	2.256
30	1.281	1.281
40	.731	.732
50	.687	.687
60	.894	.894
70	1.107	1.107
80	1.235	1.235
90	1.286	1.287
100	1.293	1.294
110	1.282	1.282
120	1.268	1.269
130	1.261	1.261
140	1.258	1.258
150	1.266	1.266
160	1.285	1.284
170	1.306	1.304
180	1.328	1.327

and the cross sections for different values of the varied ℓ-value are compared. The cross sections are considered to have converged when an increase in the number of partial waves does not change the third significant digit. Generally, the ℓ-values were increased between two and five for this comparison. While it may appear that this procedure is inefficient and time consuming and a wiser option might be to set the ℓ-values at some arbitrarily large value, in fact this is not feasible since computer time increases dramatically with the number of partial waves. Round-off and truncation errors can effect the cross sections significantly if the ℓ-values become too large.

The initial trials for the appropriate ℓ-values were based on the calculation for E_i = 256.5 eV. With these parameters, the program took more than four hours of central processor time to execute, which exceeded the maximum amount of computer time available. These trial values resulted in over four million subroutine calls in the amplitude coefficient calculators alone. Consequently, lower estimates had to be for the ℓ-values. Using the above mentioned technique, the following optimum maximum ℓ-values were found: $\ell_i = 50$, $\ell_c = 20$ and $\ell_s = 9$ for the direct case, and $\ell_i = 30$ for the exchange case. Comparisons justifying these values are shown in the tables in Appendix E.

The optimum value for ℓ_s in the exchange case was found to be fourteen, but such a high value resulted in

program execution times which exceeded the available time. It was necessary, therefore, to accept lesser accuracy to decrease the computer time. The maximum value used for ℓ_s in the exchange case was six. This value introduced approximately a 2% error into the exchange amplitude.

Using these ℓ-values, triple differential cross sections were calculated for comparison with the results of Beatty et al.[14] The kinematic parameters used for these calculations are as follows:

1) E_i = 100 eV, E_s = 5 eV, θ_f = 20°

2) E_i = 105 eV, E_s = 10 eV, θ_f = 20°

3) E_i = 125 eV, E_s = 30 eV, θ_f = 20°

4) E_i = 165 eV, E_s = 70 eV, θ_f = 20°

The cross sections were calculated for θ_s between 0° and 180° in steps of 1°; and for Φ_s from 0° to 180° in steps of 3°. It is not necessary to calculate Φ_s from 360° to 180° as it is a mirror image of Φ_s from 0° to 180°, as shown by Madison et al.[13] The results of these calculations are shown in Figures 3 through 6. The solid curve corresponds to this distorted wave calculation, the dashed curve represents the CPBA cross sections calculated by Geltman,[11] and the dotted curve corresponds to the PWBA cross sections which are calculated from an available program, and the large dots are the experimental results.

In Figures 3 through 6, the cross sections are plotted in units of $a_0^2/sr^2/Ry$, where a_0 is the Bohr radius, sr is the angular unit steradians, and Ry is the energy unit Rydberg. The kinematic parameters for figure three are as follows: the incident electron energy is 100 eV, the faster final state electron is observed at an angle of 20° in the scattering plane, and a 5 eV slower electron is detected. Cross sections are presented for a cone about q of half angle 45° for various azymuthal angles on the cone between 0° and 180°, as shown in Figure 2. The cone is centered on the momentum transfer direction with $\Phi=0$ corresponding to the half of the scattering plane containing the scattered fast electron, and $\Phi=180°$ corresponding to the other half. For this case it is seen that the PWBA amplitude is much too large and the CPBA grossly overpredicts the asymmetrical behavior of the data, while the DWA not only has the correct basic shape, but the amplitude does not leave the range of error of the experimental points. In Figure 4, E_i and E_s both have been incremented by 5 eV while the other kinematic parameters remain the same. The CPBA is in better agreement with the experimental data at smaller angles while at larger angles the DWA is closer. The PWBA is again too large. In Figure 5, E_i and E_s are both incremented by another 20 eV, while the half angle of the cone is decreased to 30°. Here it may be seen that the DWA predicts the shape of the experimental data while the CPBA does not. Finally in

Figure 2. Sketch of the coordinate system for electron ionization with the Z axis oriented along the axis of momentum transfer.

Figure 2

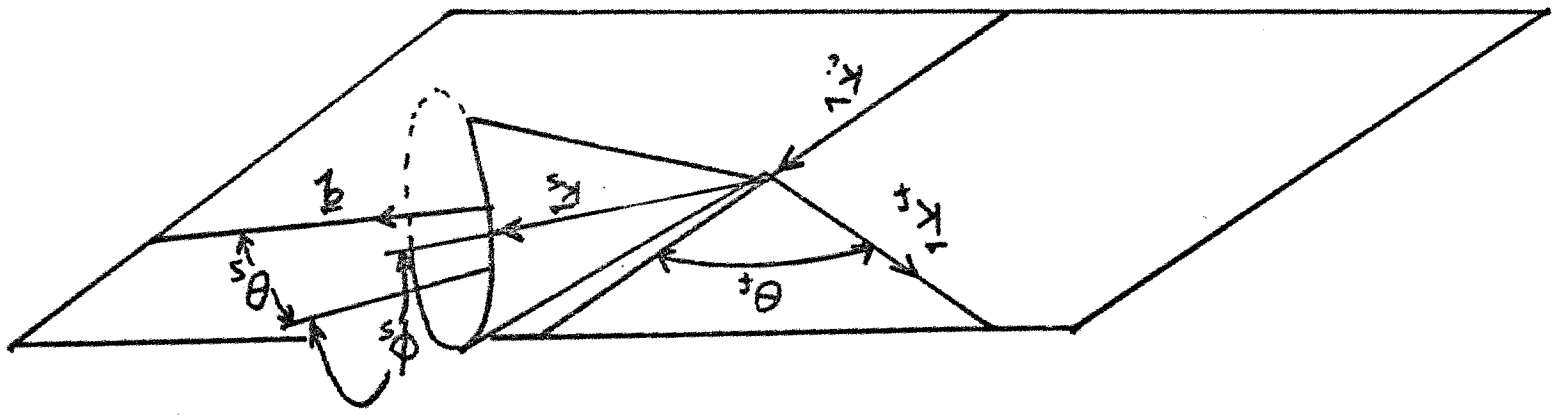

Figure 3. Triple differential cross sections for 100 eV electron impact ionization of helium in units of $a_o^2/Sr^2/Ry$. The experimental data are those of Beatty, et al., the solid curve is the present DWA calculation; the dotted curve is the PWBA calculation and the dashed curve is the CPBA calculation. The angle of observation of the faster electron, θ_f, is 20° and the energy of the slower electron, E_s, is 5 eV. The cross sections are for Φ=0 to 180° for a cone of half angle θ_s=45°.

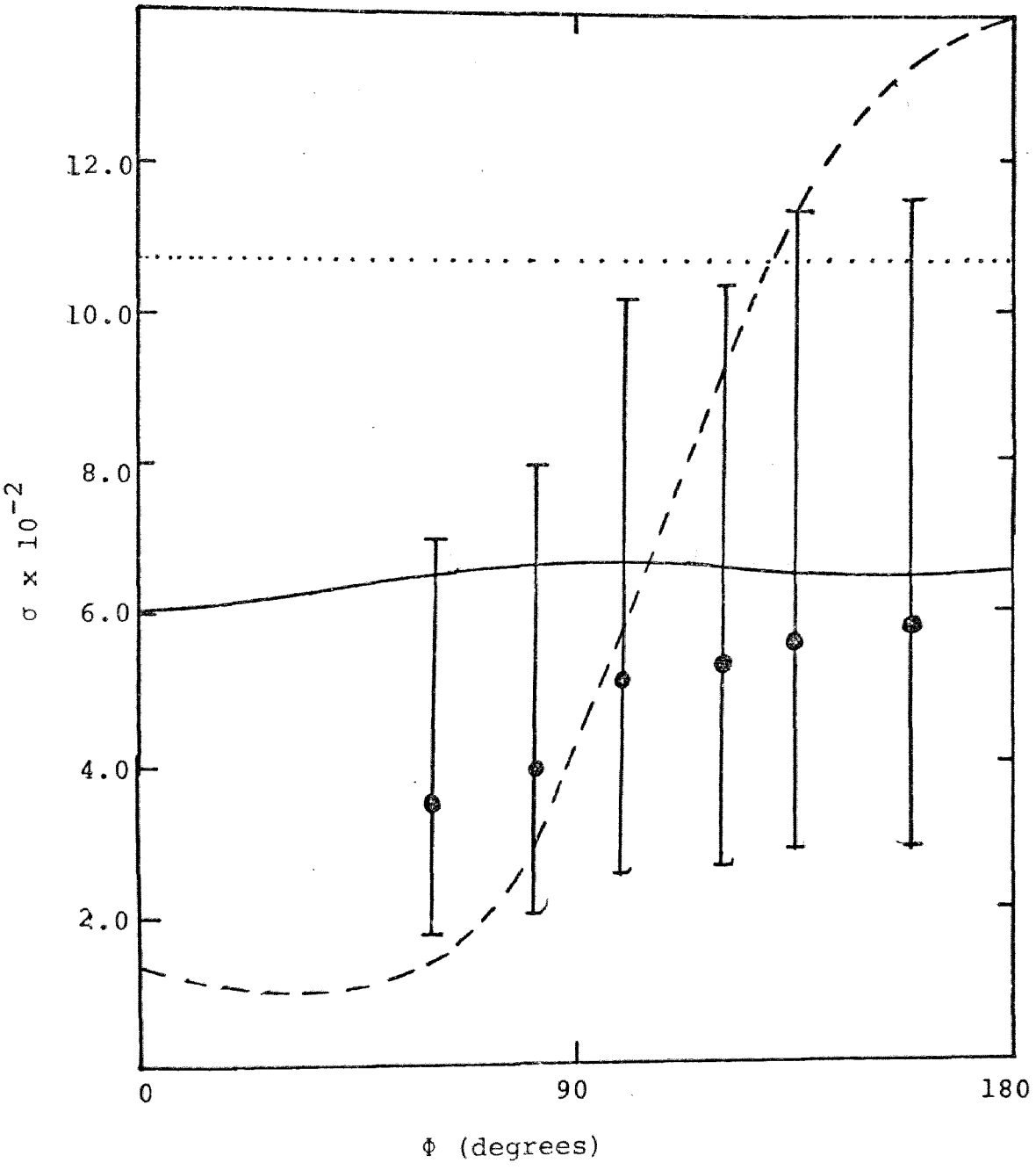

Figure 3

Figure 4. Same as Figure 3 except E_i=105 eV and E_s=10 eV.

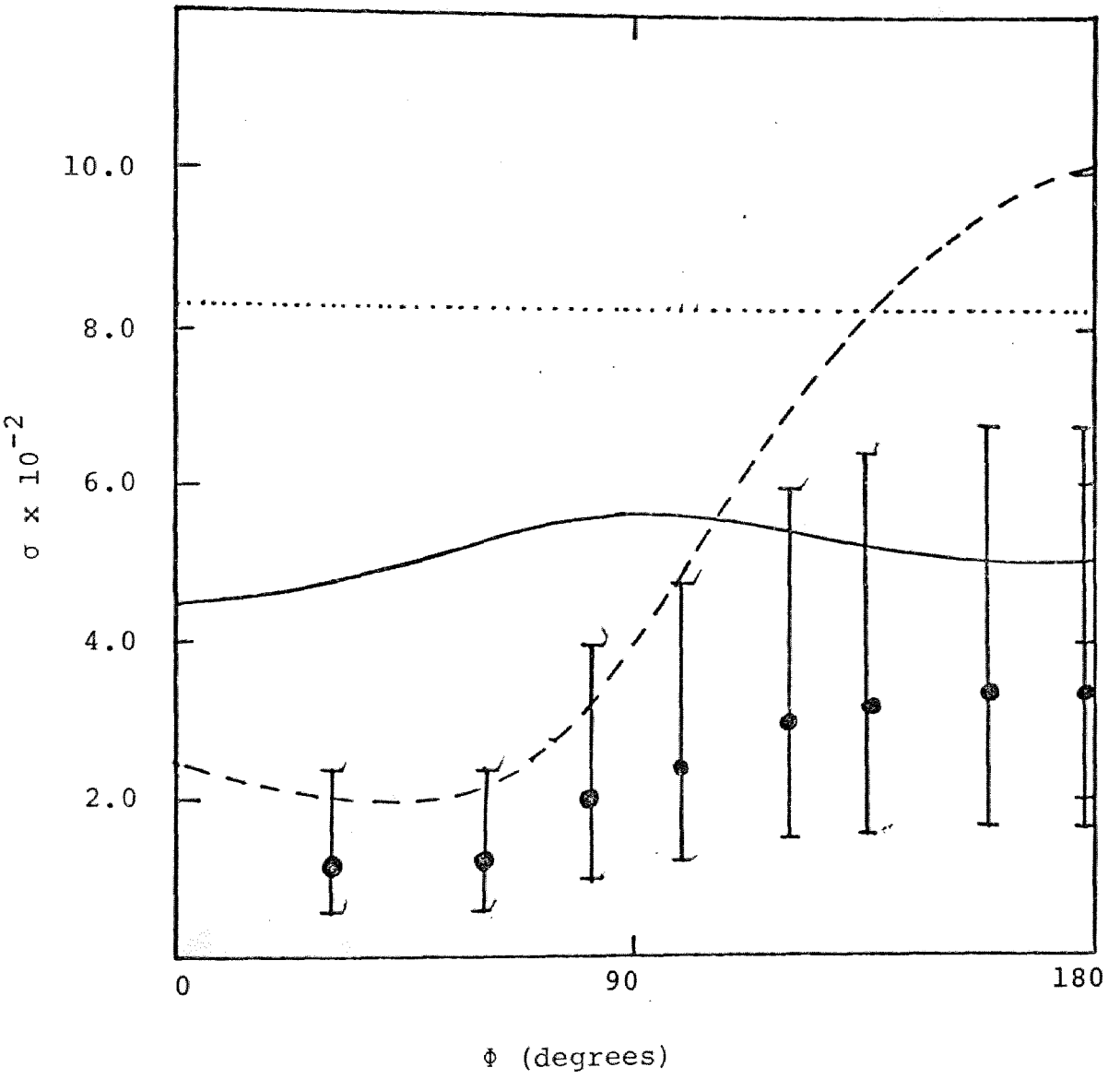

Figure 4

Figure 5. Same as Figure 3 except E_i=125 eV, E_s=30 eV, and the cone is now centered about θ_s=30°.

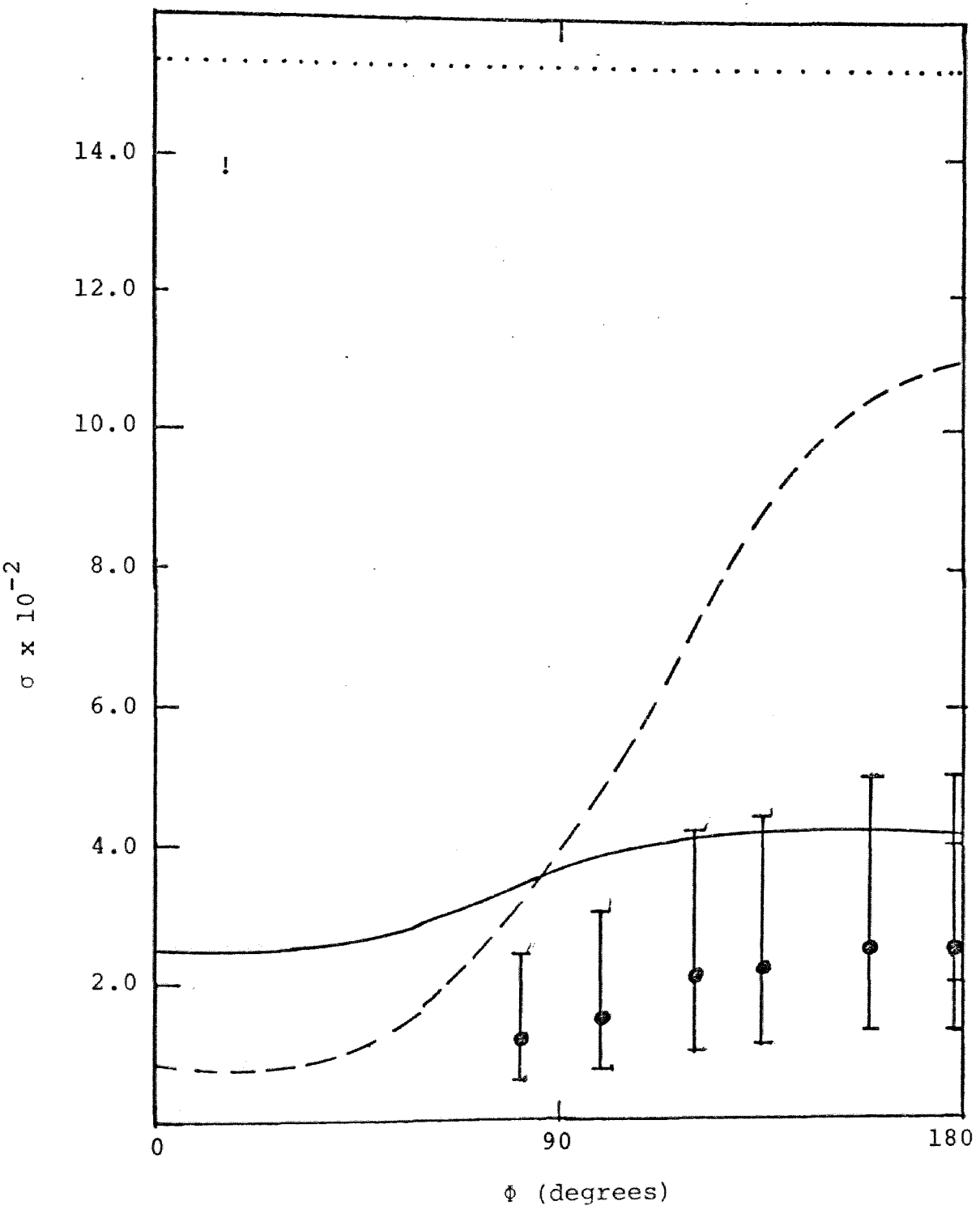

Figure 5

Figure 6. Same as Figure 3 except E_i=165 eV, E_s=70 eV, and the cone is now centered about θ_s=25°.

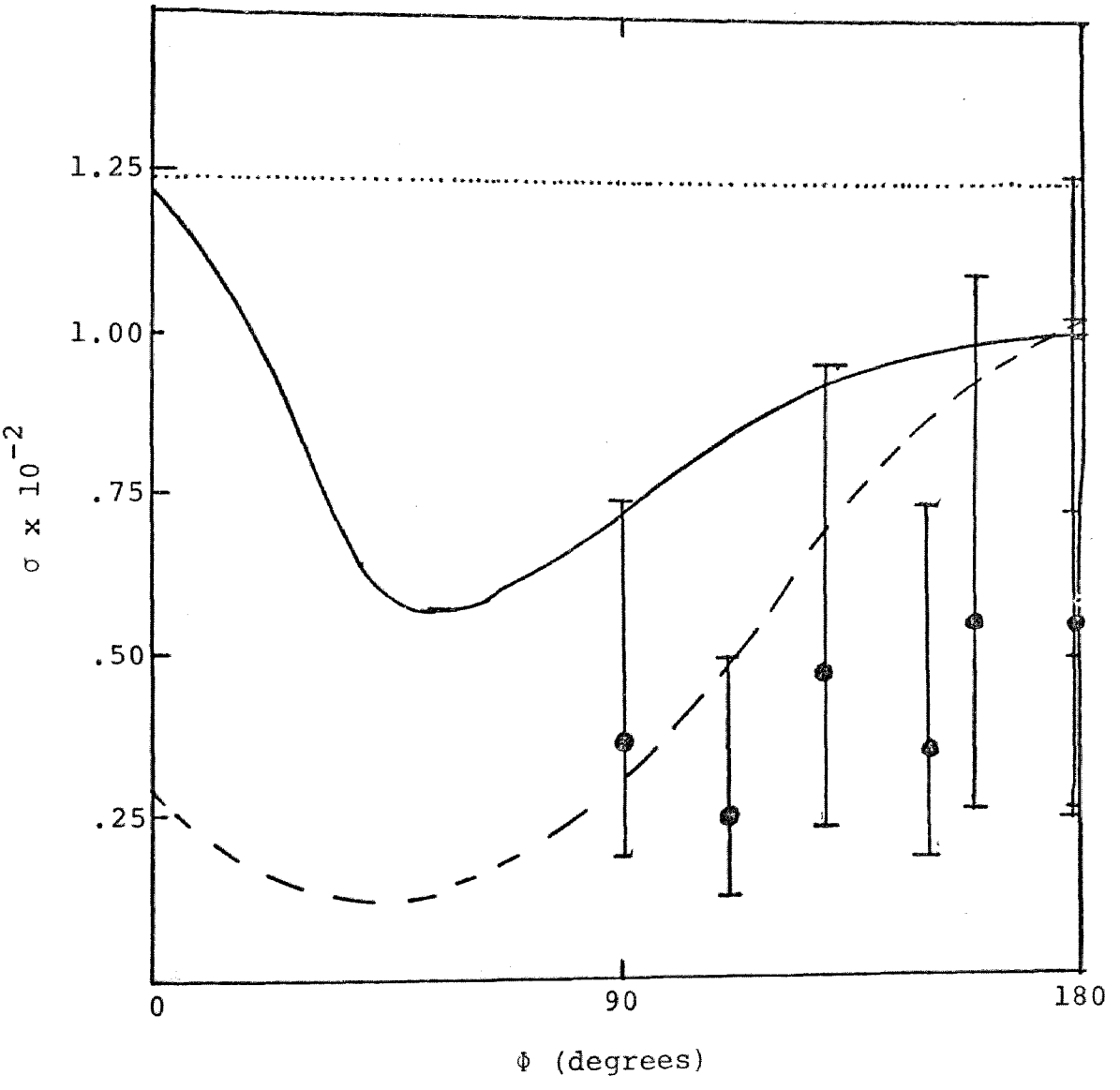

Figure 6

Figure 6, E_i and E_s are both incremented by another 40 eV while the half angle of the cone is decreased to 25°. In this case the CPBA is in better agreement with the experimental data than the DWA.

The azymuthal symmetry of the PWBA for Z along $\overline{q}$ is reflected by the constant cross section as a function of Φ_s. The CPBA predicts a major asymmetry in the cross sections with a maximum near Φ=180°. The DWA, on the other hand, is smaller in magnitude and predicts only a small asymmetry in the cross sections similar in shape to the experimental results. Since the experimental results are accurate to within a factor of two, the DWA affords better agreement with the experiment than either the CPBA or the PWBA simply because it predicts the asymmetry of the cross sections without overestimating the amplitude.

Chapter 4

CONCLUSIONS

In conclusion, it may be noted from Madison et al.[13] that the DWA was superior to the CPBA which was superior to the PWBA in reproducing experimental results for higher energies of the incident electron. In this thesis, both the DWA and the experimental data exhibit only a small asymmetry in a cone about the momentum transfer direction, a feature of the PWBA. This observation is interesting for two reasons: first, one would not expect the results to be Born-like for incident energies in this range. Secondly, it is interesting to note that while the magnitude of the DWA is significantly different from the PWBA the behavior of the two approximations are similar. Surprisingly, the simple PWBA once again appears to be qualitatively correct in its prediction of the physics even though the PWBA magnitude may not be reliable.

REFERENCES

1. H. Ehrhardt, K. H. Hesselbacher, K. Jung, and K. Willmann, J. Phys. B 5, 1559 (1973).

2. H. Ehrhardt, K. H. Hesselbacher, K. Jung, M. Schulz, and K. Willmann, J. Phys. B 5, 2107 (1972).

3. H. Ehrhardt, K. H. Hesselbacher, K. Jung, E. Schubert, and K. Willmann, J. Phys. B 7, 69 (1974).

4. K. Jung, E. Schubert, H. Ehrhardt, and D. A. L. Paul, J. Phys. B 9, 75 (1976).

5. S. T. Hood, I. E. McCarthy, P. J. O. Teubner, and E. Weigold, Phys. Rev. A 8, 2494 (1973).

6. E. Weigold, Second International Conference on Inner Shell Ionization Phenomena, Invited Papers, Freiburg, W-Germany, 1976, p. 367.

7. A. Salin, J. Phys. B 6, 134 (1973).

8. V. L. Jacobs, Phys. Rev. A 10, 499 (1974).

9. W. D. Robb, S. P. Roundtree, and T. Burnett, Phys. Rev. A 11, 1193 (1975).

10. T. Burnett, S. P. Roundtree, G. Doolen, and W. D. Robb, Phys. Rev. A 13, 626 (1976).

11. S. Geltman, J. Phys. B 7, 1994 (1974).

12. K. L. Baluja and H. S. Taylor, J. Phys. B 9, 829 (1976).

13. D. H. Madison, R. V. Calhoun, and W. N. Shelton, to be published.

14. E. C. Beatty, K. H. Hesselbacher, S. P. Hong, and J. H. Moore, to be published.

15. M. E. Rose, Elementary Theory of Angular Momentum (New York: Wiley, 1967), Chapter III.

16. C. F. Fischer, Computer Physics Communications, 1 (1969), 151-166.

APPENDIX A

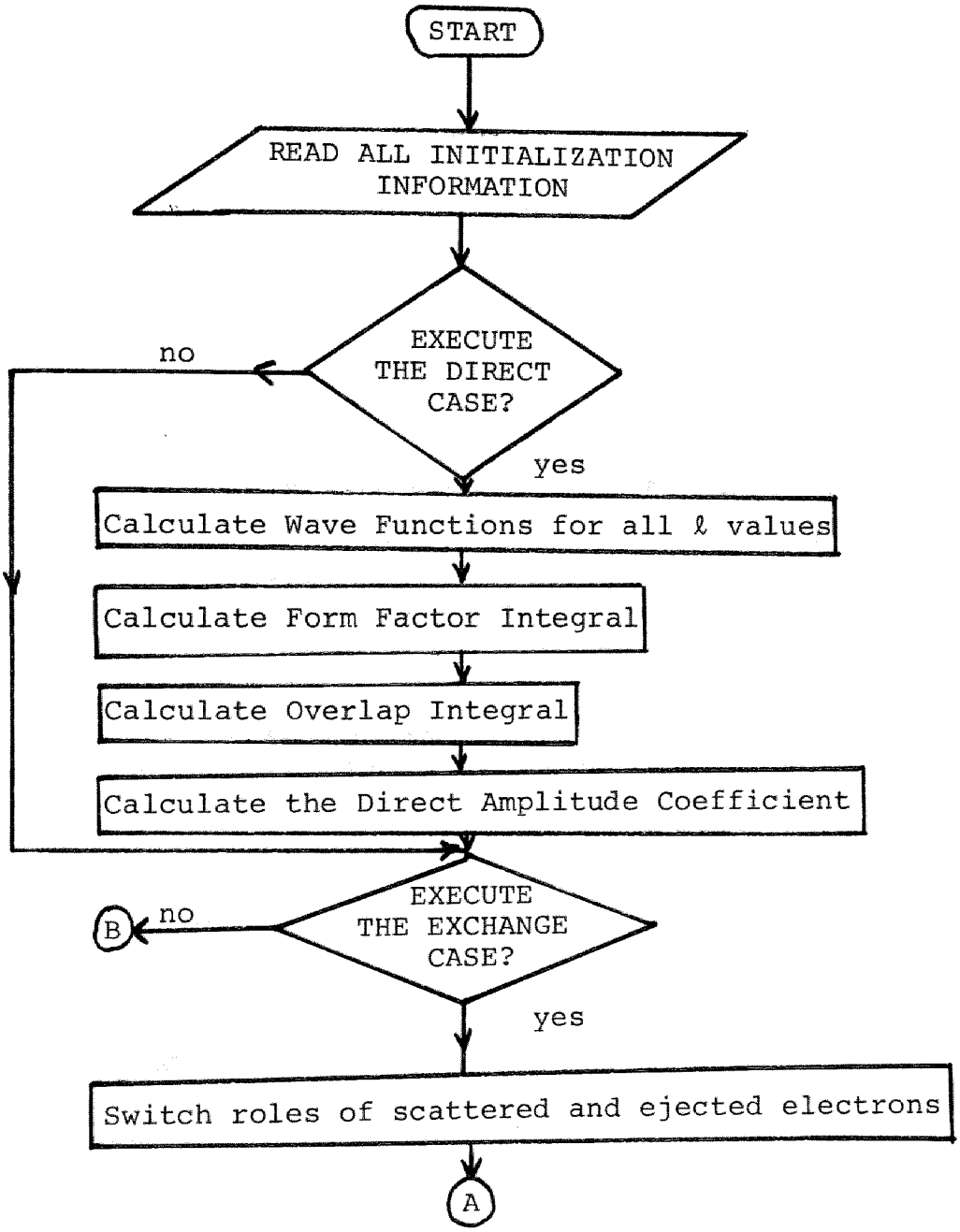
START
READ ALL INITIALIZATION INFORMATION
EXECUTE THE DIRECT CASE?
no
yes
Calculate Wave Functions for all ℓ values
Calculate Form Factor Integral
Calculate Overlap Integral
Calculate the Direct Amplitude Coefficient
EXECUTE THE EXCHANGE CASE?
B
no
yes
Switch roles of scattered and ejected electrons
A

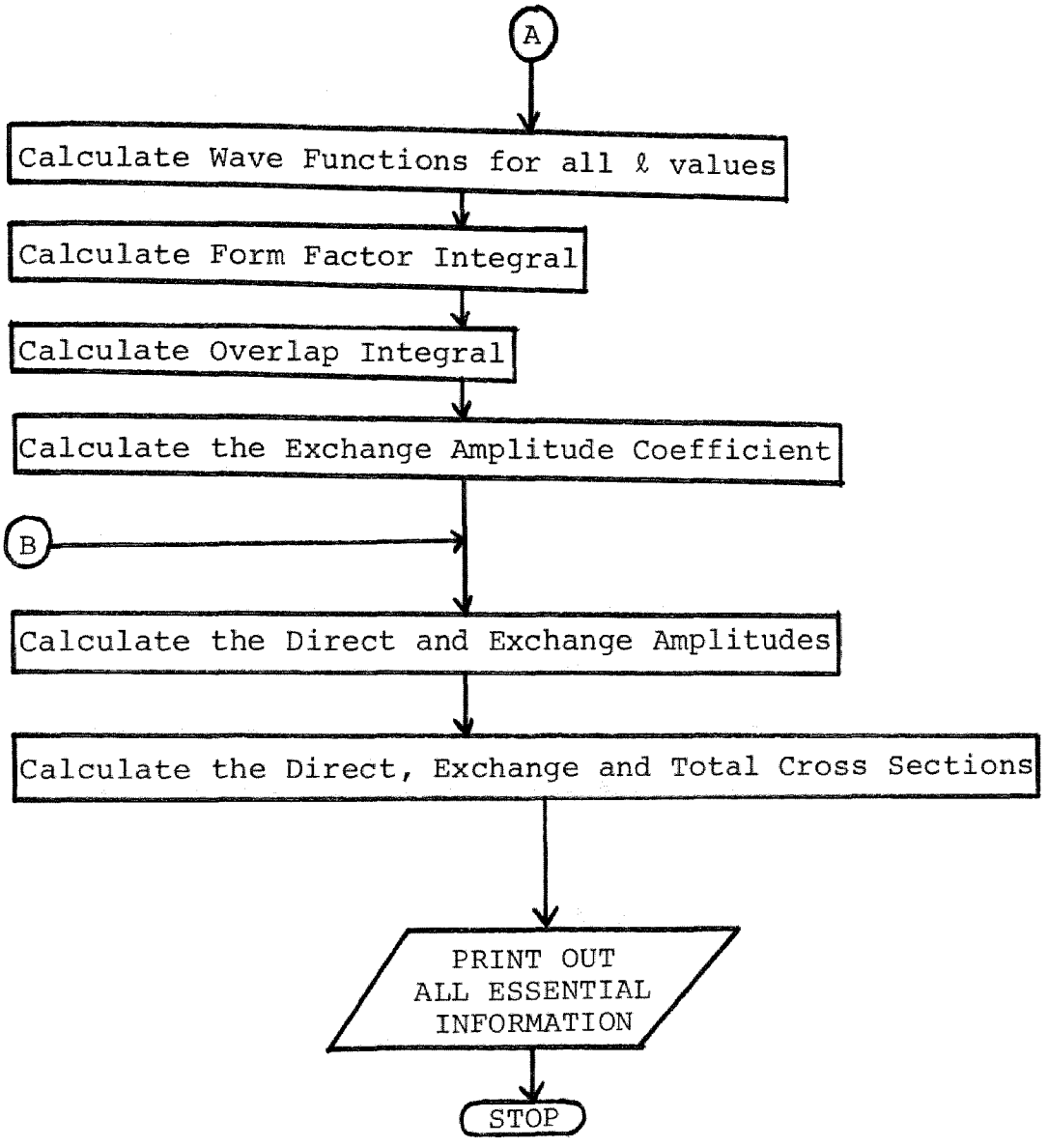
A
Calculate Wave Functions for all ℓ values
Calculate Form Factor Integral
Calculate Overlap Integral
Calculate the Exchange Amplitude Coefficient
B
Calculate the Direct and Exchange Amplitudes
Calculate the Direct, Exchange and Total Cross Sections
PRINT OUT
ALL ESSENTIAL
INFORMATION
STOP

APPENDIX B

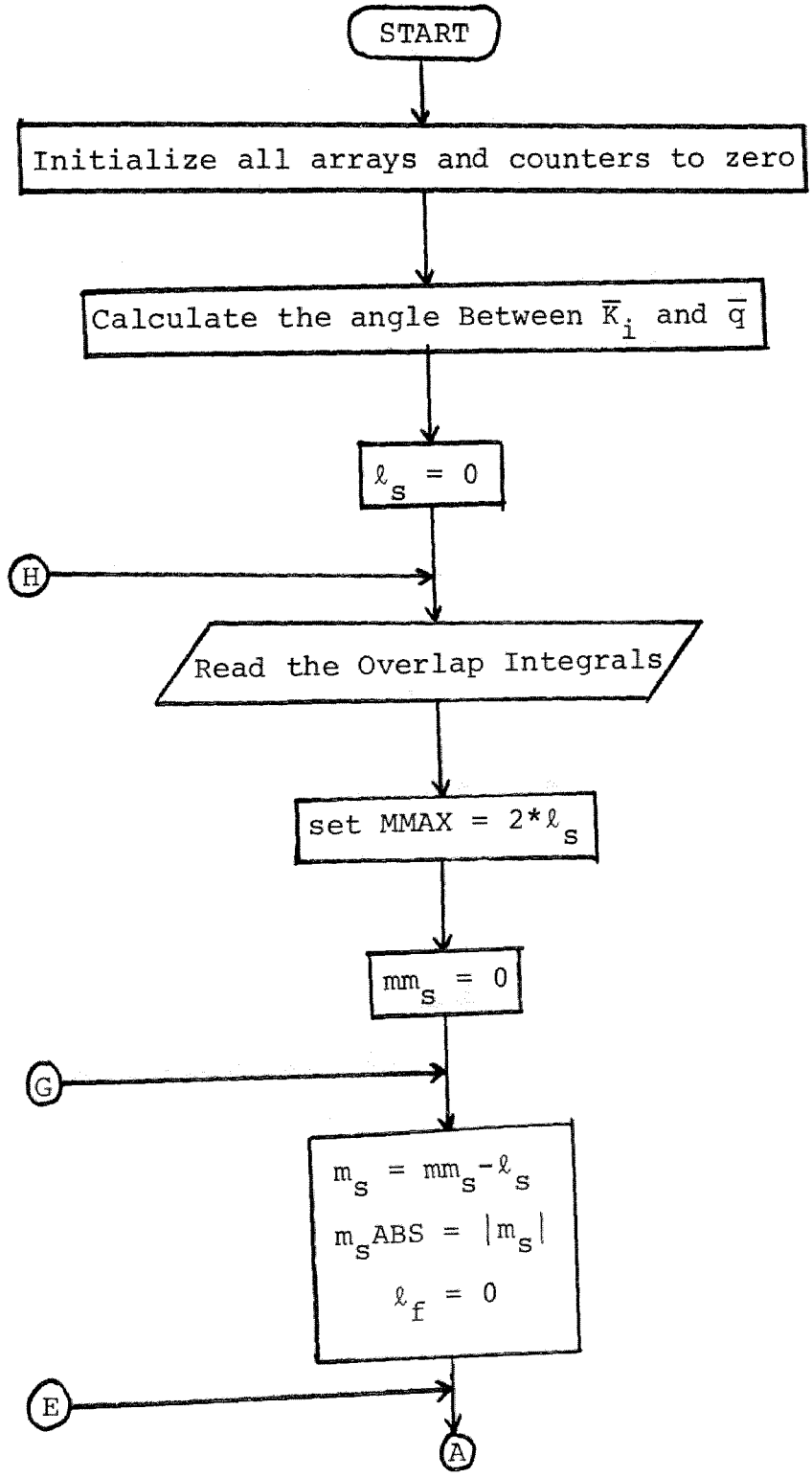
START
Initialize all arrays and counters to zero
Calculate the angle Between $\overline{K}_i$ and $\overline{q}$
$\ell_s = 0$
H
Read the Overlap Integrals
set MMAX = $2*\ell_s$
$mm_s = 0$
G
$m_s = mm_s - \ell_s$
$m_s ABS = |m_s|$
$\ell_f = 0$
E
A

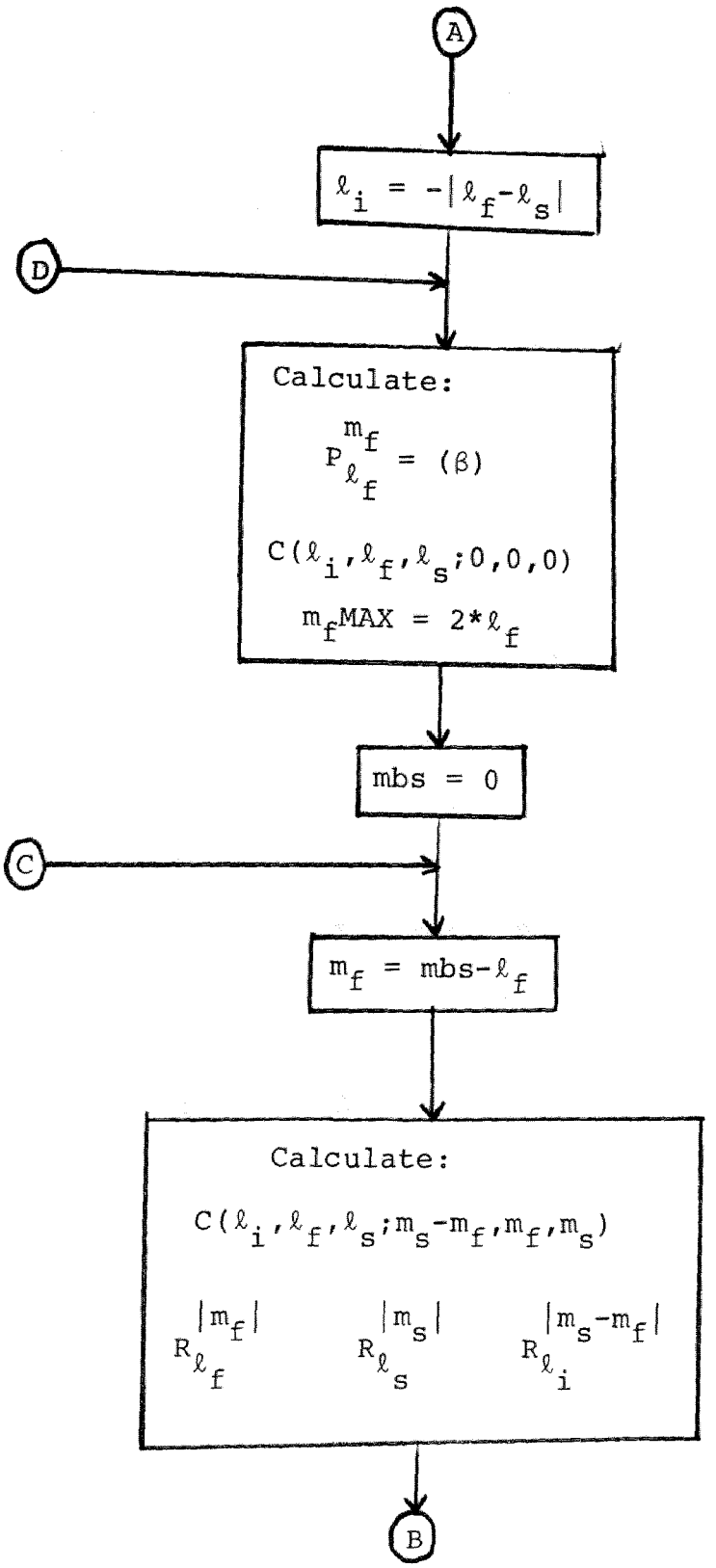
A
$\ell_i = -|\ell_f - \ell_s|$
D
Calculate:
$P_{\ell_f}^{m_f} = (\beta)$
$C(\ell_i, \ell_f, \ell_s; 0, 0, 0)$
$m_f MAX = 2 * \ell_f$
mbs = 0
C
$m_f = mbs - \ell_f$
Calculate:
$C(\ell_i, \ell_f, \ell_s; m_s - m_f, m_f, m_s)$
$R_{\ell_f}^{|m_f|}$
$R_{\ell_s}^{|m_s|}$
$R_{\ell_i}^{|m_s - m_f|}$
B

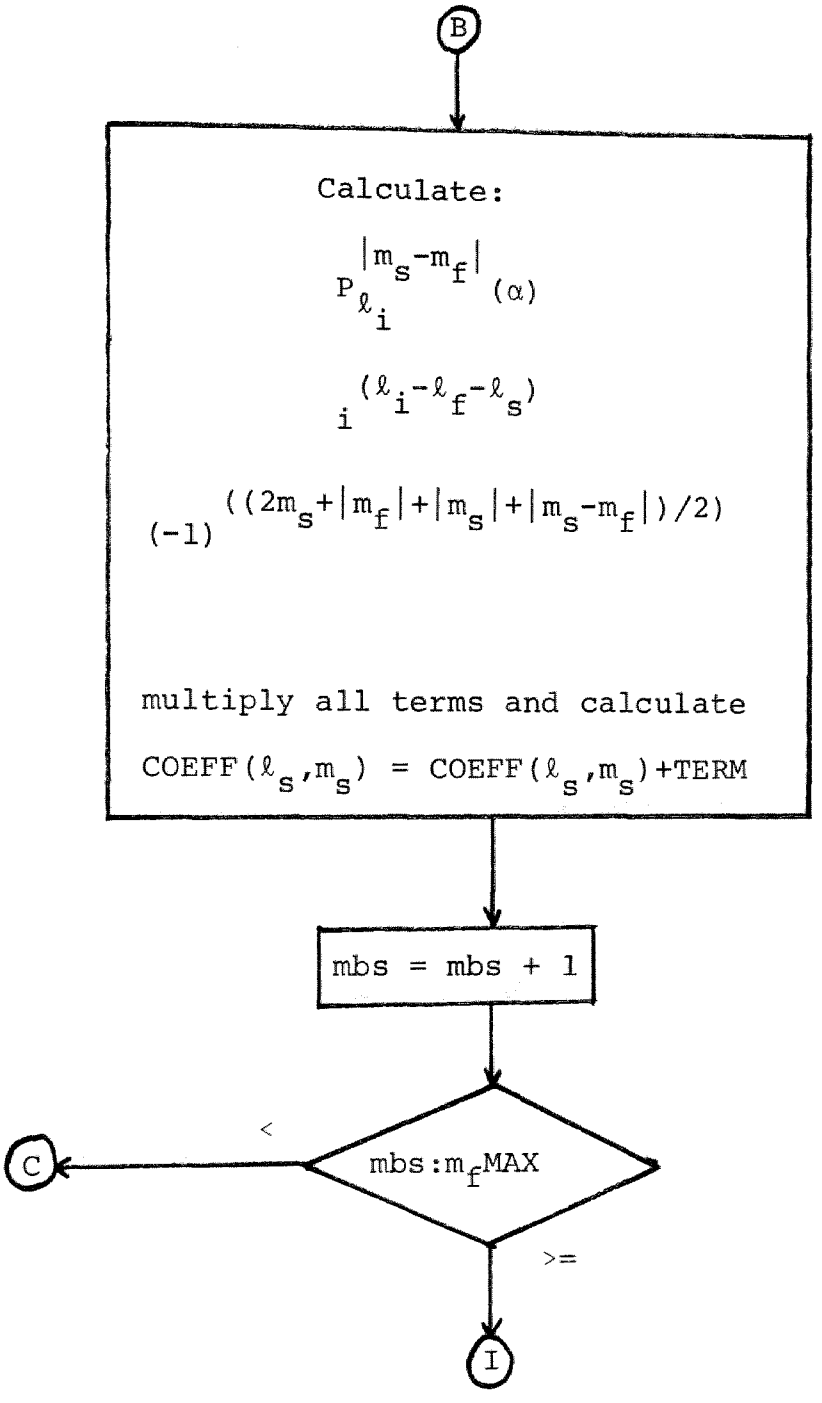
B
Calculate:
$P_{\ell_i}^{|m_s-m_f|}(\alpha)$
$i^{(\ell_i-\ell_f-\ell_s)}$
$(-1)^{((2m_s+|m_f|+|m_s|+|m_s-m_f|)/2)}$
multiply all terms and calculate
COEFF(ℓ_s,m_s) = COEFF(ℓ_s,m_s)+TERM
mbs = mbs + 1
mbs:m_fMAX
<
>=
C
I

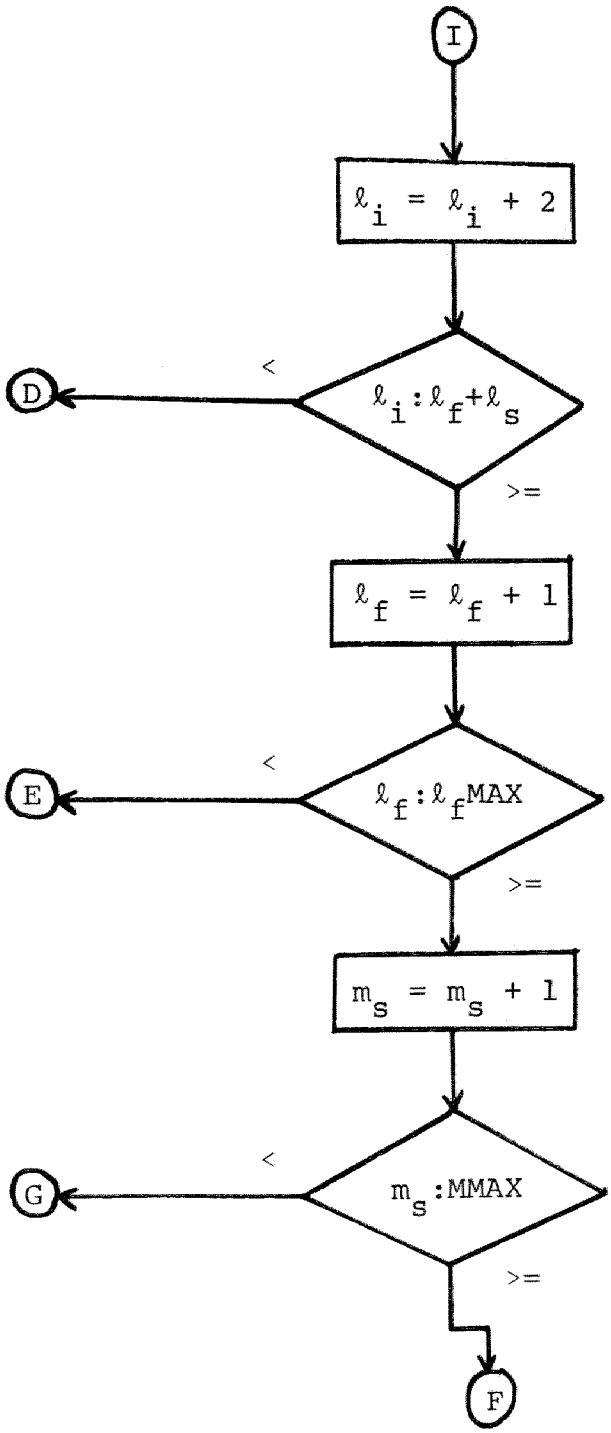
I
$\ell_i = \ell_i + 2$
<
$\ell_i : \ell_f + \ell_s$
D
>=
$\ell_f = \ell_f + 1$
<
$\ell_f : \ell_f MAX$
E
>=
$m_s = m_s + 1$
<
$m_s : MMAX$
G
>=
F

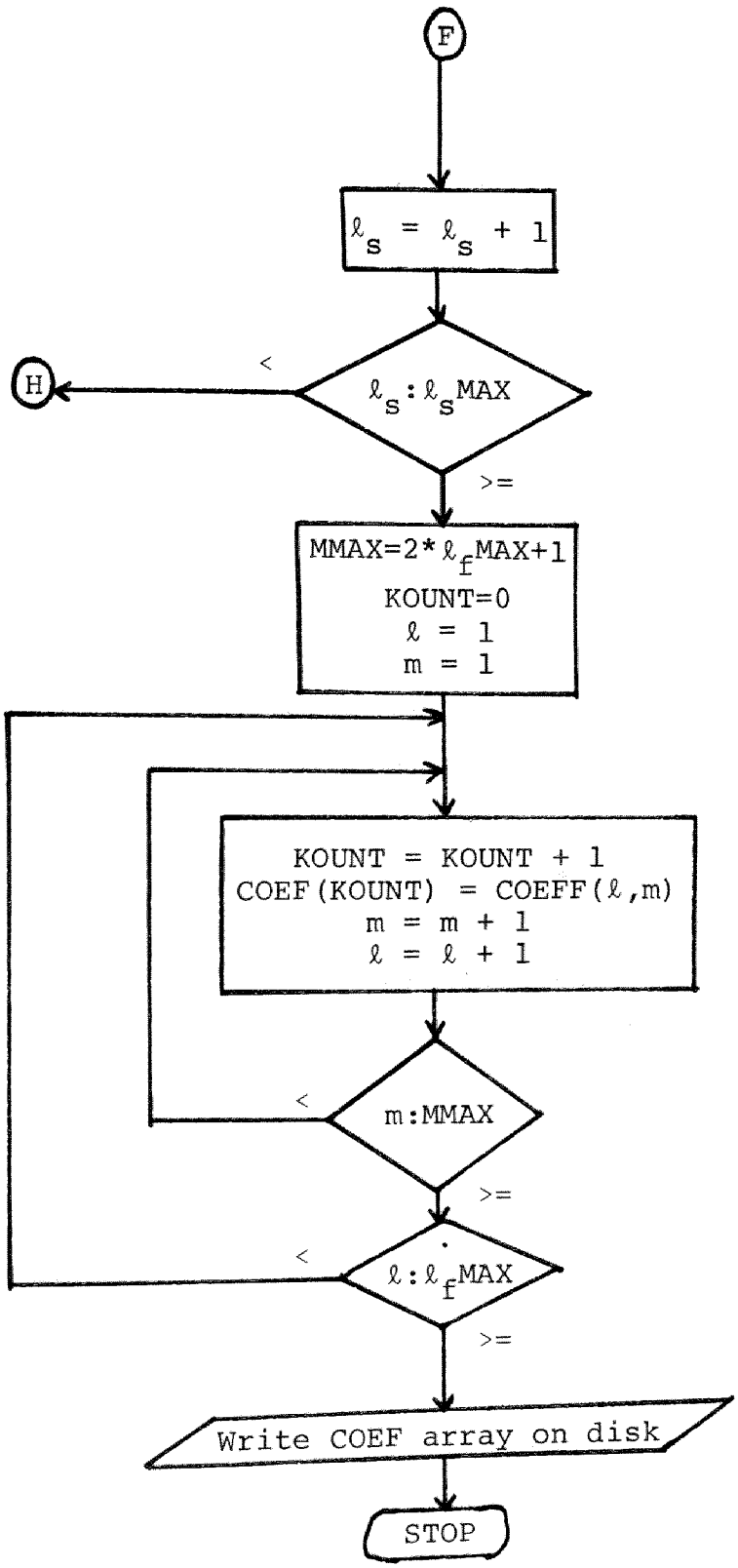
F
$\ell_s = \ell_s + 1$
$\ell_s : \ell_s MAX$
<
H
>=
MMAX=2*ℓ_fMAX+1
KOUNT=0
ℓ = 1
m = 1
KOUNT = KOUNT + 1
COEF(KOUNT) = COEFF(ℓ,m)
m = m + 1
ℓ = ℓ + 1
m:MMAX
<
>=
$\ell : \ell_f MAX$
<
>=
Write COEF array on disk
STOP

APPENDIX C

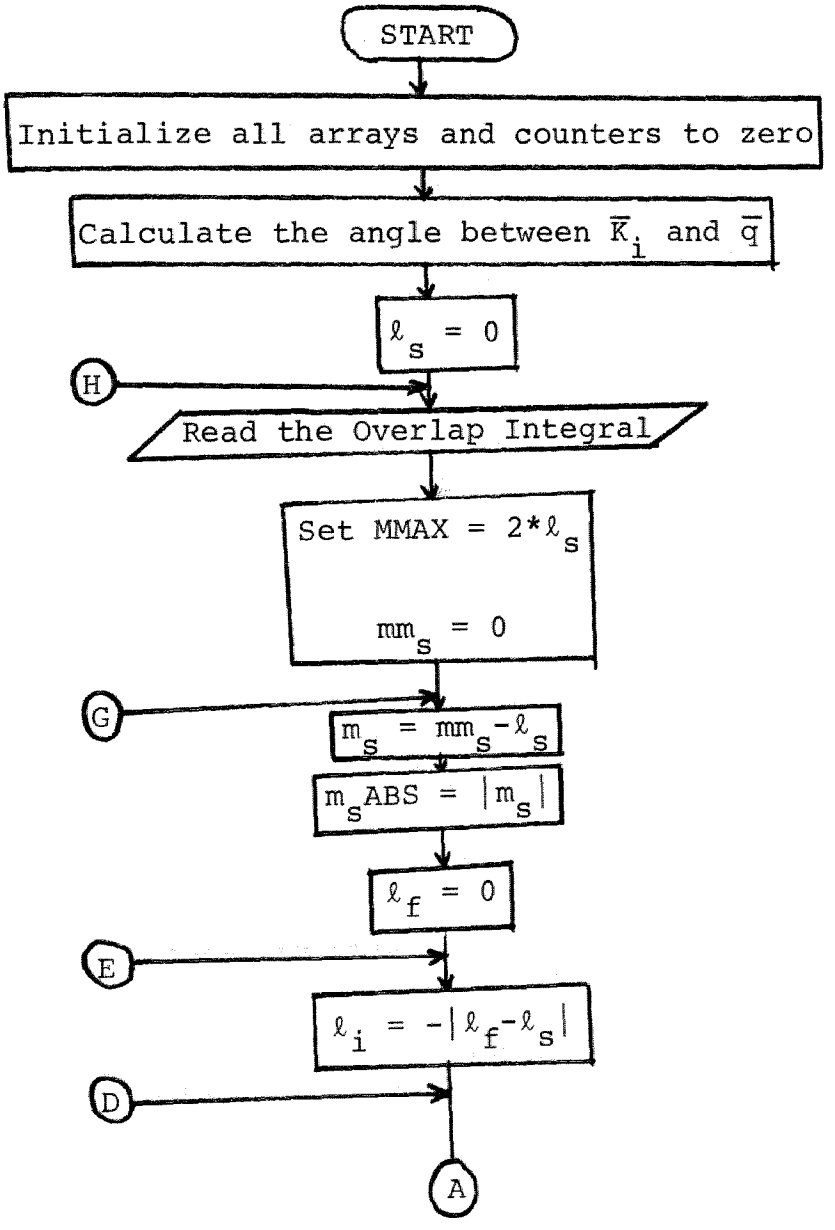
START
Initialize all arrays and counters to zero
Calculate the angle between $\overline{K}_i$ and $\overline{q}$
$\ell_s = 0$
H
Read the Overlap Integral
Set MMAX = $2*\ell_s$
$mm_s = 0$
G
$m_s = mm_s - \ell_s$
$m_s ABS = |m_s|$
$\ell_f = 0$
E
$\ell_i = -|\ell_f - \ell_s|$
D
A

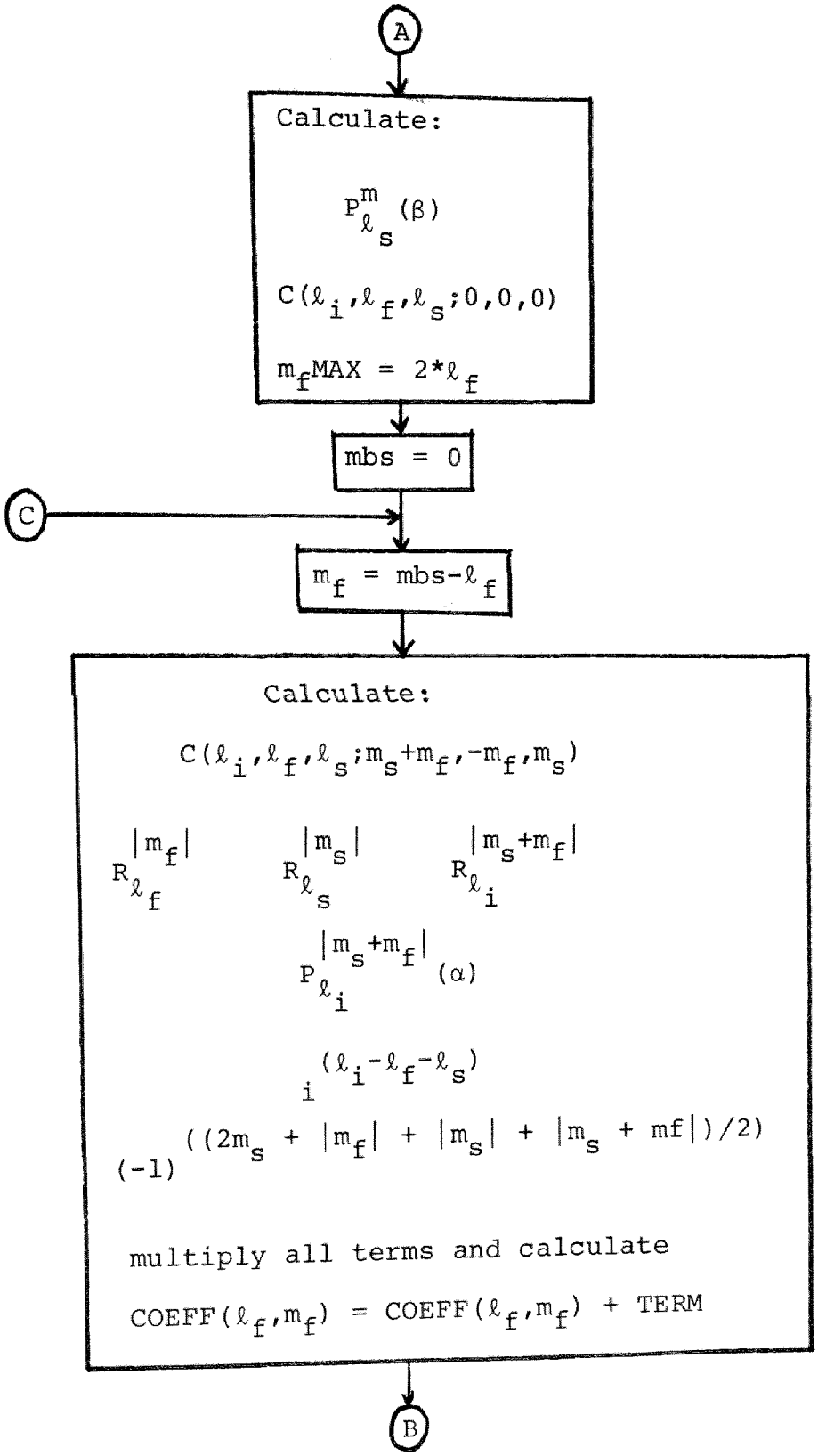
A
Calculate:
$P_{\ell_s}^{m}(\beta)$
$C(\ell_i,\ell_f,\ell_s;0,0,0)$
$m_f MAX = 2*\ell_f$
mbs = 0
C
m_f = mbs-ℓ_f
Calculate:
$C(\ell_i,\ell_f,\ell_s;m_s+m_f,-m_f,m_s)$
$R_{\ell_f}^{|m_f|}$ $R_{\ell_s}^{|m_s|}$ $R_{\ell_i}^{|m_s+m_f|}$
$P_{\ell_i}^{|m_s+m_f|}(\alpha)$
$i^{(\ell_i-\ell_f-\ell_s)}$
$(-1)^{((2m_s + |m_f| + |m_s| + |m_s + mf|)/2)}$
multiply all terms and calculate
COEFF(ℓ_f,m_f) = COEFF(ℓ_f,m_f) + TERM
B

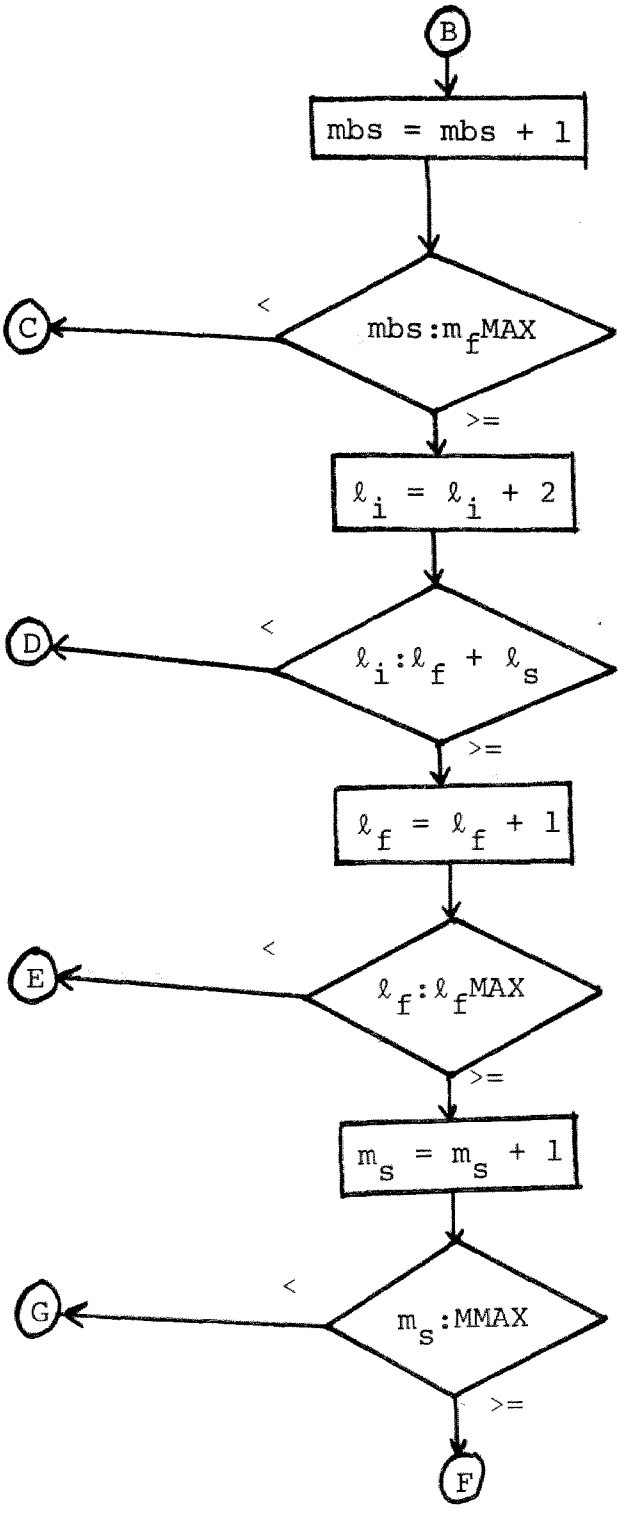
B
mbs = mbs + 1
mbs : m_fMAX
<
C
>=
$\ell_i = \ell_i + 2$
$\ell_i : \ell_f + \ell_s$
<
D
>=
$\ell_f = \ell_f + 1$
$\ell_f : \ell_f$MAX
<
E
>=
$m_s = m_s + 1$
m_s : MMAX
<
G
>=
F

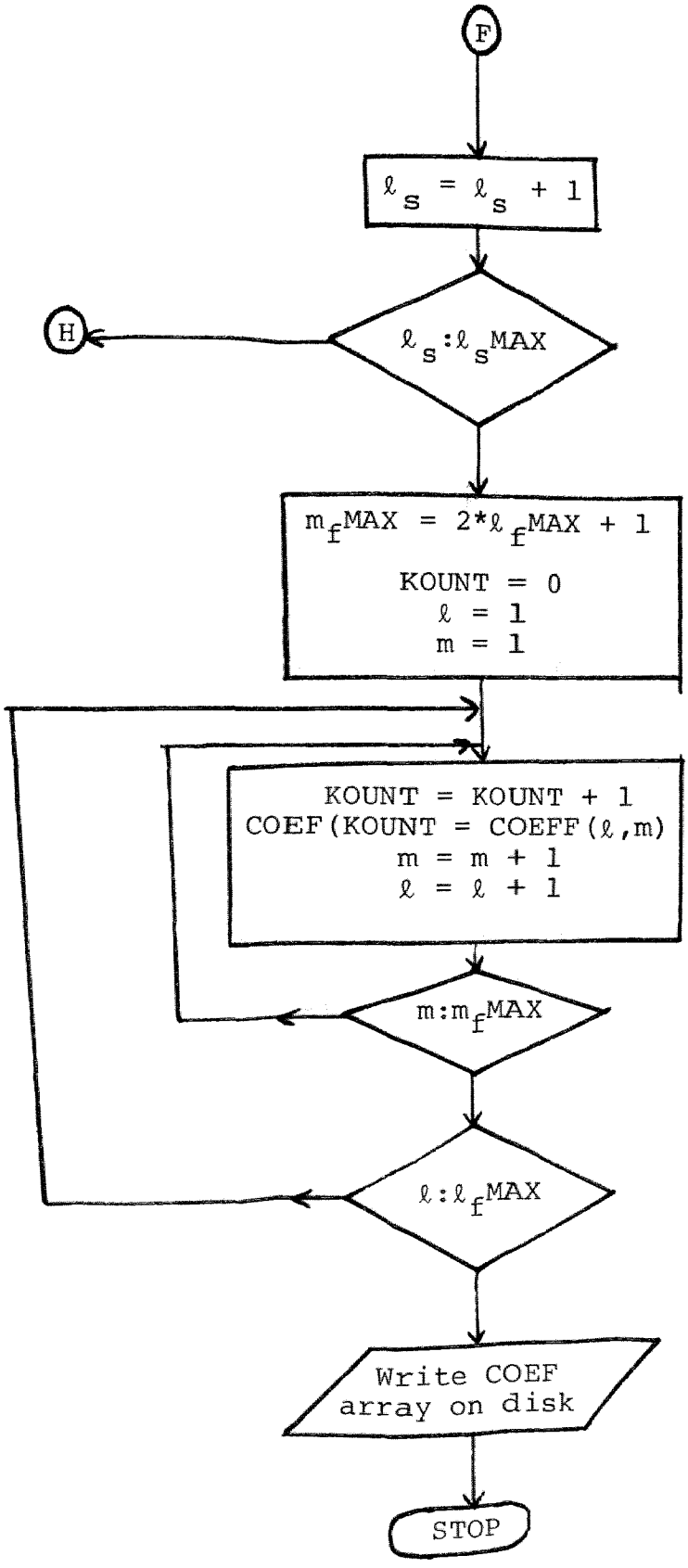
F
$\ell_s = \ell_s + 1$
H
$\ell_s : \ell_s MAX$
$m_f MAX = 2*\ell_f MAX + 1$
KOUNT = 0
ℓ = 1
m = 1
KOUNT = KOUNT + 1
COEF(KOUNT = COEFF(ℓ,m)
m = m + 1
ℓ = ℓ + 1
$m : m_f MAX$
$\ell : \ell_f MAX$
Write COEF array on disk
STOP

APPENDIX D

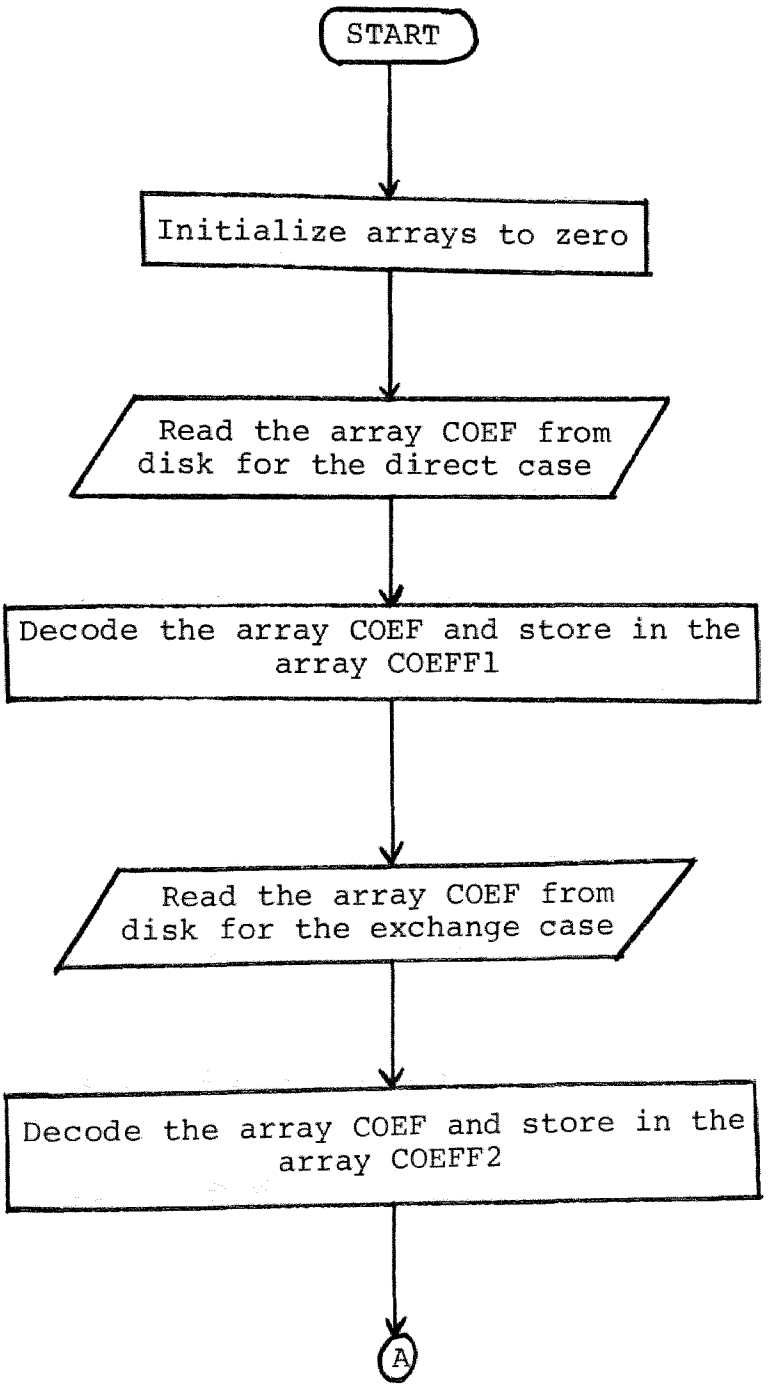
START
Initialize arrays to zero
Read the array COEF from disk for the direct case
Decode the array COEF and store in the array COEFF1
Read the array COEF from disk for the exchange case
Decode the array COEF and store in the array COEFF2
A

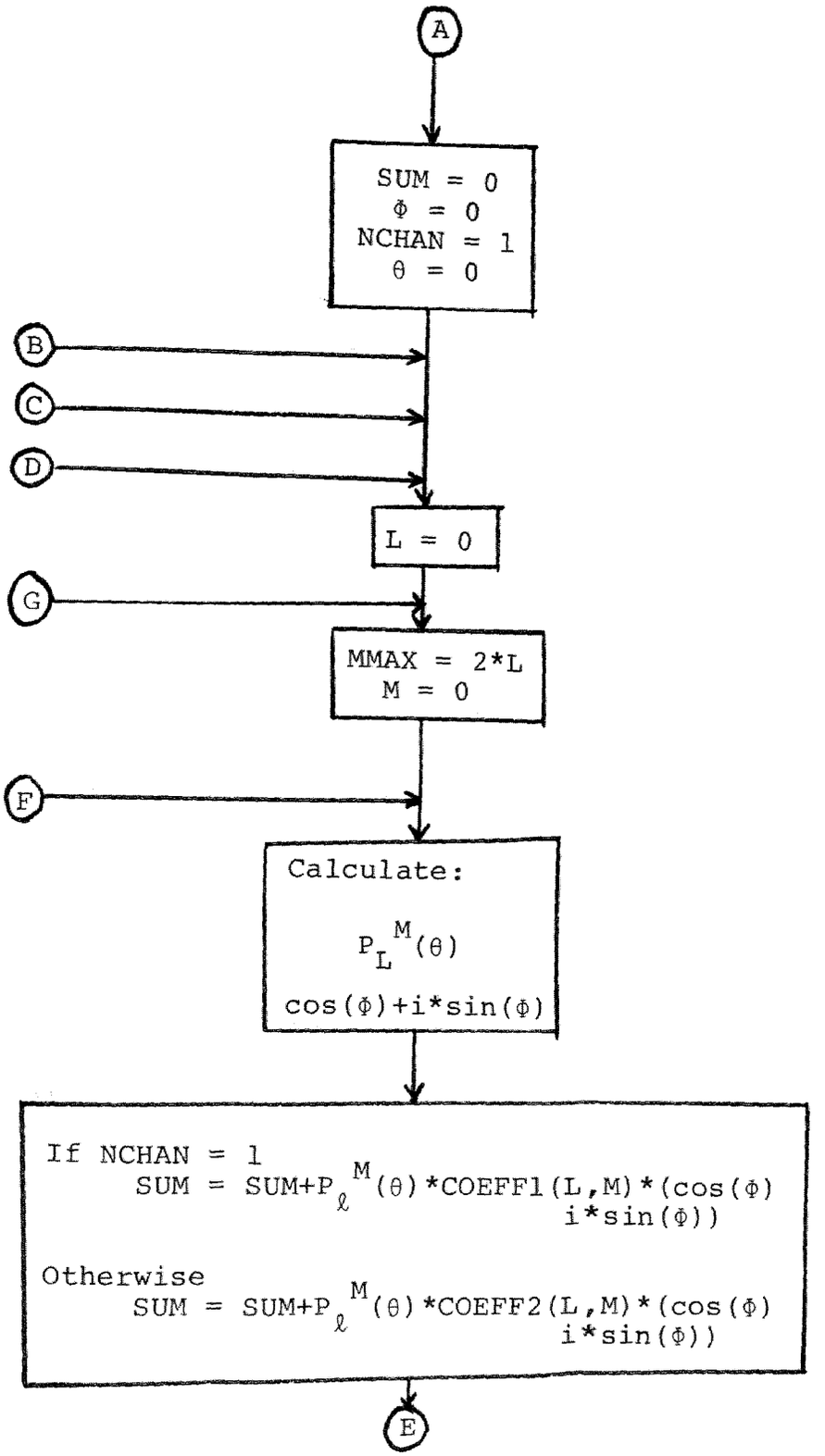
A
SUM = 0
Φ = 0
NCHAN = 1
θ = 0
B
C
D
L = 0
G
MMAX = 2*L
M = 0
F
Calculate:
$P_L^M(\theta)$
cos(Φ)+i*sin(Φ)
If NCHAN = 1
SUM = SUM+$P_\ell^M(\theta)$*COEFF1(L,M)*(cos(Φ)
i*sin(Φ))
Otherwise
SUM = SUM+$P_\ell^M(\theta)$*COEFF2(L,M)*(cos(Φ)
i*sin(Φ))
E

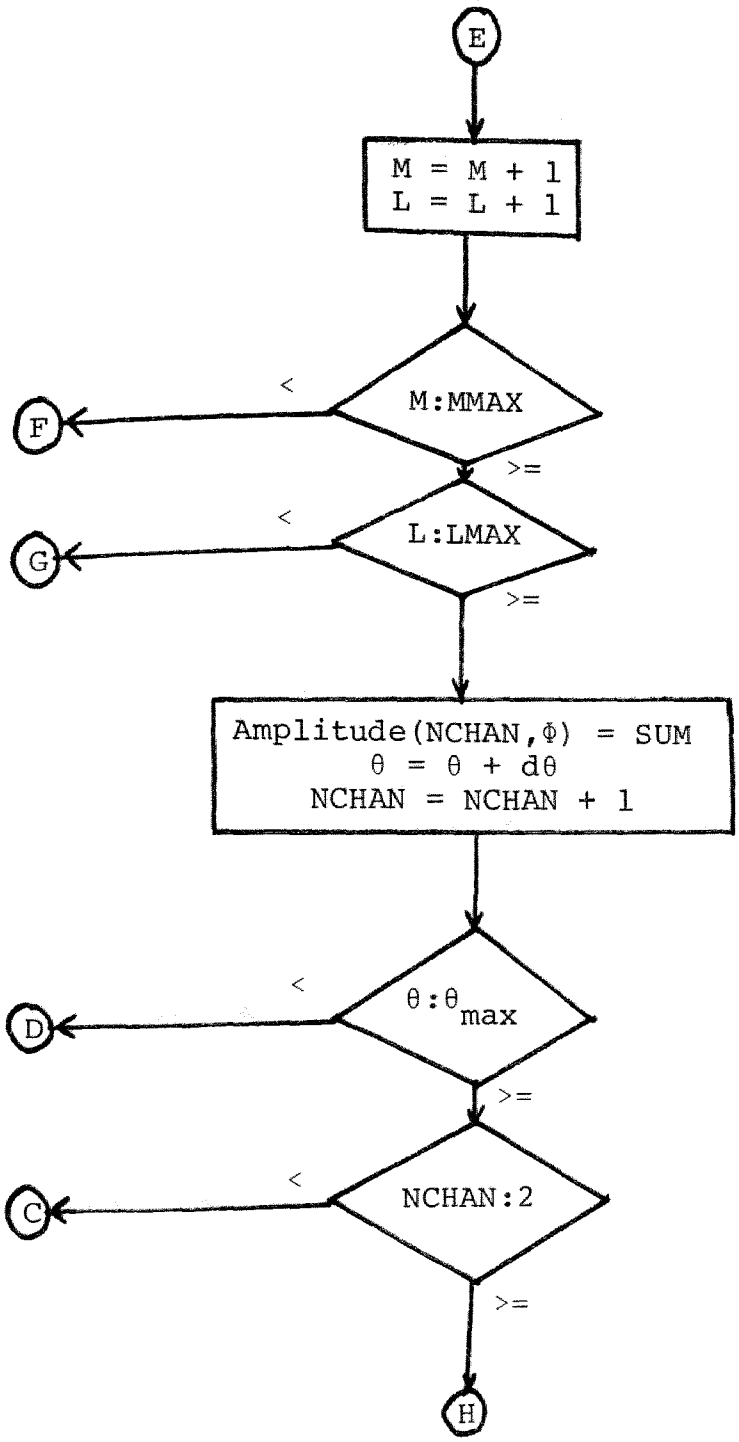
E
M = M + 1
L = L + 1
M:MMAX
<
F
>=
L:LMAX
<
G
>=
Amplitude(NCHAN,Φ) = SUM
θ = θ + dθ
NCHAN = NCHAN + 1
θ:θmax
<
D
>=
NCHAN:2
<
C
>=
H

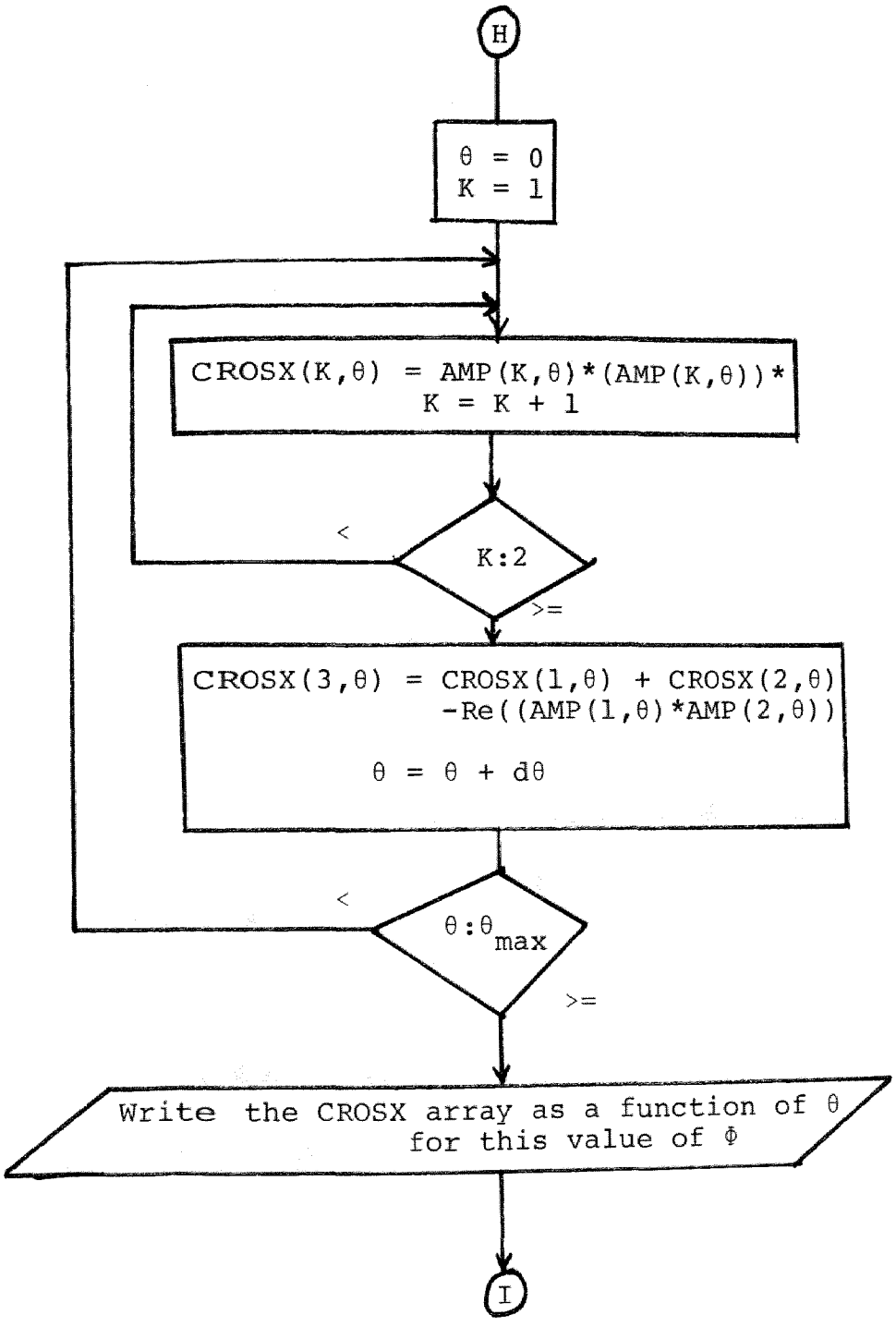
H
θ = 0
K = 1
CROSX(K,θ) = AMP(K,θ)*(AMP(K,θ))*
K = K + 1
<
K:2
>=
CROSX(3,θ) = CROSX(1,θ) + CROSX(2,θ)
-Re((AMP(1,θ)*AMP(2,θ))
θ = θ + dθ
<
θ:θmax
>=
Write the CROSX array as a function of θ
for this value of Φ
I

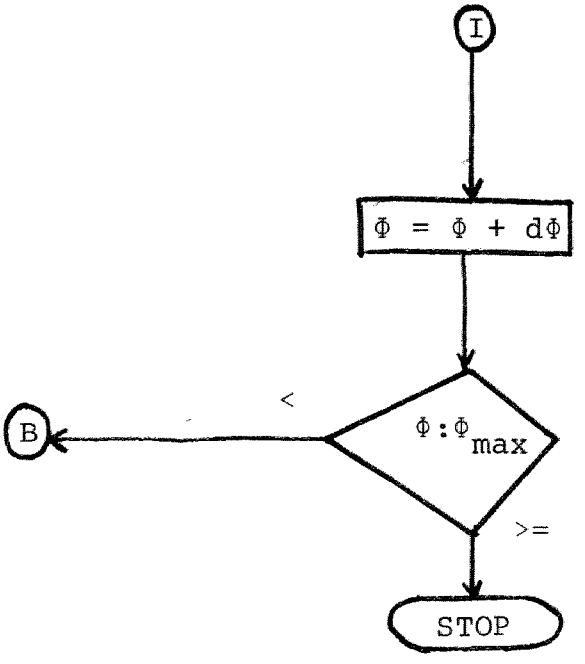
I
Φ = Φ + dΦ
Φ : Φmax
<
>=
B
STOP

APPENDIX E

Table 2

Table of Cross Sections for Z Along $\bar{q}$ in Units of $a_o^2/Sr^2/Ry$, For Comparison of Partial Wave Parameters.

DIRECT $L_f=40$ $L_i=50$ $\Phi=0$

θ	$L_s=7$	$L_s=9$	$L_s=11$
0	2.045×10^{-1}	2.040×10^{-1}	2.039×10^{-1}
30	.906	.908	.908
60	.467	.467	.467
90	.598	.598	.598
120	.618	.618	.618
150	.661	.662	.662
180	.705	.701	.701

DIRECT $L_s=9$ $L_i=50$ $\Phi=0$

θ	$L_f=20$	$L_f=30$
0	2.021×10^{-1}	2.021×10^{-1}
30	.897	.897
60	.471	.471
90	.604	.604
120	.618	.618
150	.657	.657
180	.695	.695

DIRECT $L_f=40$ $L_s=7$ $\Phi=0$

θ	$L_i=75$	$L_i=50$	$L_i=30$
0	2.045×10^{-1}	2.045×10^{-1}	2.035×10^{-1}
30	.906	.906	.897
60	.467	.467	.472
90	.598	.598	.608
120	.619	.619	.622
150	.661	.661	.656
180	.705	.705	.700

Table 2 (Continued)

EXCHANGE	$L_s=8$ $\Phi=0$	
θ	$L_f=30$	$L_f=40$
0	7.546×10^{-3}	7.546×10^{-3}
30	9.063	9.066
60	2.568	2.569
90	2.719	2.718
120	2.883	2.883
150	3.382	3.382
180	3.964	3.964